Acknowledgments

The work of the first author was supported in part by the Naticnal Transportation Safety Board under Research Grant RA-3-013 to the second author.

References

[1]Aircraft Accident Report—Northwest Airlines, Inc., McDonnell Douglas DC-9-82, N312RC, Detroit Metropolitan Wayne County Airport, Romulus, MI, Aug. 16, 1987; National Transportation Safety Board, 1988.

[2]Aircraft Accident Report—Delta Air Lines, Inc., Boeing 727-232, N473DA, Dallas–Fort Worth International Airport, TX, Aug. 31, 1988; National Transportation Safety Board, 1989.

[3]Airworthiness Standards: Transport Category Airplanes, 14CFR Pt. 25, Jan. 1994, Paragraph 25.103.

[4]Flight Test Guide for Certification of Transport Category Aircraft, U.S. Dept. of Transportation, FAA, Advisory Circular 25-7, 1986.

[5]Ligum, S. U., Scripnichenko, L. A., Chulsky, A. V., Shishmareyv, S. I., and Yurovsky, S. I., *Aerodinamica Samoleta Tu-154*, Transport, Moscow, 1977.

[6]Stevens, B. L., and Lewis, F. L., *Aircraft Control and Simulation*, Wiley, New York, 1992.

[7]Nelson, R. C., *Flight Stability and Automatic Control*, McGraw–Hill, New York, 1989.

Approximate Formula for the Frequencies of a Rotating Timoshenko Beam

V. T. Nagaraj*
Hindustan Aeronautics Ltd.,
Bangalore 560017, India

Introduction

IT is well known that shear deformation and rotary inertia can have an important influence on the frequencies of nonrotating beams. This influence can be especially significant for beams made of advanced composite materials because of the high ratio of Young's modulus to the shear modulus. For nonrotating beams, these effects can be modeled by Timoshenko's equations for which exact solutions are available.[1,2]

An approximate formula for the frequencies and mode shapes of rotating uniform cantilever Euler–Bernoulli beams is given by Peters.[3] The expression given by Peters is simple and very accurate for the entire blade stiffness range. It gives accurate results for the fundamental frequency as well as for the overtones.

In this Note, the formula of Peters is modified, based on analogy, to include the influence of shear deformation and rotary inertia. Though the theoretical basis is not formal, comparison with exact results shows that the present expressions give surprisingly accurate results for frequencies, even for very short beams.

Approximate Expression for the Frequency

The differential equation of motion for the flapping vibrations of a rotating beam including the influence of shear deformation and rotary inertia is[4]

$$(1 + \delta\alpha p)W'''' + 3\delta\alpha pW''' - [1 - \varepsilon\delta(\lambda + \alpha)] \times (\alpha p'W' + \lambda W) + [\delta\lambda + (\varepsilon + \varepsilon\delta\alpha p)(\lambda + \alpha) - \alpha(p - 3\delta p'')]W'' = 0 \tag{1}$$

In Eq. (1), W is the total lateral displacement that is the sum of the bending and shearing displacements. The other quantities are

$$\xi = \frac{x}{L}, \quad \alpha = \frac{mL^4\Omega^2}{EI}, \quad \lambda = \frac{mL^4\omega^2}{EI}, \quad \delta = \frac{EI}{GKAL^2}$$
$$\varepsilon = \frac{I_z}{mL^2}, \quad p = \frac{1}{2}(1 - \xi^2), \quad ()' = \frac{\partial()}{\partial\xi} \tag{2}$$

where x is the axial coordinate, L is the length of the beam, m is the mass per unit length, EI is the bending rigidity, A is the area of cross section of the beam, G is the shear modulus, I_z is the mass moment of inertia in flap, and K is the Timoshenko shear coefficient that accounts for the influence of shear deformation,[5] and δ and ε are the shear deflection coefficient and rotary inertia coefficient, respectively.[4]

The equation of motion of a rotating Euler–Bernoulli beam is obtained from Eq. (1) by setting δ and ε equal to zero as

$$W'''' - \alpha(pW)' - \lambda W = 0 \tag{3}$$

For a rotating Euler–Bernoulli cantilever beam, Peters obtained an approximate formula for the nth (nondimensional) frequency as

$$\lambda_n = n(2n - 1)\alpha + \lambda^0_{NR} + F\sqrt{\alpha}\tan^{-1}\left[\frac{A_{nn} - n(2n - 1)}{F}\sqrt{a}\right] \tag{4}$$

where λ^0_{NR} = nth frequency of nonrotating beam:

$$F = \frac{\sqrt{2}}{\pi}(4n - 1)\left[\frac{(2n)!}{n!(n - 1)!_2}\frac{1}{2^{2n-1}}\right] \tag{5}$$

$$A_{nn} = \frac{1}{2}\int_0^1 (1 - \xi^2)\phi_n'^2\, d\xi \tag{6}$$

In Eq. (6), ϕ_n is the nth mode shape of a nonrotating uniform cantilever beam. Equation (4) represents an approximation valid for all stiffnesses and frequencies. The first term is the rotating string frequency (for large α or small EI). In the third term A_{nn} is the centrifugal stiffness for small α, and F is the correction to λ of the order of $(1/\sqrt{\alpha})$.

Since the equations for free vibrations in lead–lag of a Euler–Bernoulli beam can be obtained by replacing λ_n by $(\lambda_n + 1)$ (Ref. 3), Eq. (4) can be used to obtain the lead–lag frequency with λ_n replaced by $(1 + \lambda_{n\,\text{Lead-Lag}})$.

To include the influence of δ and ε in Eq. (4), the following reasoning is used:

1) The first term in Eq. (4) represents the limit when stiffness tends to zero (rotating string) and is not affected by δ and ε.

2) The second term corresponds to the nonrotating frequency of the Timoshenko beam for which exact solutions are available.

Depending on the values of δ and ε, the frequencies are lower than those of corresponding Euler–Bernoulli values. In addition, the term containing $\alpha\delta p$ in Eq. (1) tends to further reduce this frequency. Hence, the second term in Eq. (4) is proposed to be replaced by

$$[1 - (\alpha\delta/2^n)]f_1\lambda^0_{NR} \tag{7}$$

Received May 25, 1994; revision received Nov. 23, 1995; accepted for publication Dec. 29, 1995.

*Additional General Manager (Design), Helicopter Design Bureau, P.O. Box 1789.

Table 1 Comparison of fundamental frequency values, $\omega/\sqrt{EI/mL^4}$

	Euler–Bernoulli		L/R = 50		L/R = 25		L/R = 10	
$\sqrt{\alpha} = \sqrt{mL^2\Omega/EI}$	Exact	Present	Exact	Present	Exact	Present	Exact	Present
0, nonrotating	3.516	3.516	3.5026	3.5026	3.4636	3.4636	3.2274	3.2274
3	4.7973	4.8066	4.7803	4.7947	4.7302	4.7402	4.4500	4.4539
6	7.3604	7.4379	7.3319	7.4261	7.2523	7.3407	6.8509	6.9291
12	13.1702	13.5721	13.1046	13.5513	12.9292	13.4138	12.1665	12.6283

Table 2 Comparison of second mode frequency values, $\omega/\sqrt{EI/mL^4}$

	Euler–Bernoulli		L/R = 50		L/R = 25		L/R = 10	
$\sqrt{\alpha} = \sqrt{mL^2\Omega/EI}$	Exact	Present	Exact	Present	Exact	Present	Exact	Present
0, nonrotating	22.0345	22.0345	21.4698	21.4698	20.0147	20.0147	14.4689	14.4689
3	23.3203	22.3188	22.7599	22.7551	21.3237	21.3060	15.9655	15.7688
6	26.8090	26.7932	26.2488	26.2243	24.8280	24.7679	19.6787	19.1459
12	37.6030	37.5155	36.9790	36.8870	35.4151	35.2872	29.3024	28.9518

Table 3 Comparison of frequencies of third mode, $\omega/\sqrt{EI/mL^4}$

	Euler–Bernoulli		L/R = 50		L/R = 25		L/R = 10	
$\sqrt{\alpha} = \sqrt{mL^2\Omega/EI}$	Exact	Present	Exact	Present	Exact	Present	Exact	Present
0, nonrotating	61.6972	61.6972	58.1498	58.1498	50.5619	50.5619	31.5025	31.5025
3	62.9850	62.9720	59.4681	59.4491	52.0499	51.9302	33.5134	33.2384
6	66.6839	66.5420	63.2386	63.0795	56.0230	55.7288	38.5785	37.8758
12	79.6145	78.7187	76.2744	75.3810	69.3360	68.3765	51.2741	52.0821

Table 4 Comparison of frequencies of fourth mode, $\omega/\sqrt{EI/mL^4}$

	Euler–Bernoulli		L/R = 50		L/R = 25		L/R = 10	
$\sqrt{\alpha} = \sqrt{mL^2\Omega/EI}$	Exact	Present	Exact	Present	Exact	Present	Exact	Present
0, nonrotating	120.9020	120.9020	109.0275	109.0275	88.1952	88.1952	47.9090	47.9090
3	122.2354	122.1947	110.4310	110.3938	89.8244	89.7439	50.1484	50.7143
6	126.1404	125.7600	114.5177	114.1630	94.5109	94.0098	56.2950	56.7234
12	141.2441	138.3231	129.3472	127.3653	110.7867	108.6921	79.0558	76.6459

where

$$f_1 = \lambda_{NR}/\lambda^0_{NR} \tag{8}$$

and λ^0_{NR} is the nondimensional frequency of nonrotating Euler–Bernoulli beam and λ_{NR} is the corresponding value for the Timoshenko beam.

3) The third term in Eq. (4) is the correction of the order of $(1/\sqrt{\alpha})$ to λ. It is proposed that for the Timoshenko beam, this term be multiplied by

$$f_2 = f_1^{1/2} \tag{9}$$

Thus, the approximate formula for the frequency of a rotating Timoshenko beam is

$$\lambda_n = n(2n-1)\alpha + \left(1 - \frac{\alpha\delta}{2^n}\right) f_1 \lambda^0_{NR} + F\sqrt{\alpha} f_2 \tan^{-1}\left[\frac{A_{nn} - n(2n-1)}{F}\,\alpha^{1/2}\right] \tag{10}$$

Comparison with Exact Values

Stafford and Giurgiutiu[4] have used the Frobenius method to solve Eq. (1). This method was used to generate the first four frequencies of rotating cantilever beams having slenderness (length-to-radius of gyration) ratios of 10, 25, and 50. The beams are assumed to have a rectangular cross section and the Timoshenko shear correction factor K is assumed to be 5/6. The ratio (E/G) is taken to be 2.6.

Tables 1–4 give a comparison of the first four frequencies for α = 0, 9, 36, and 144 for the four beams calculated by Eq. (10) and corresponding exact values. The results show very good correlation with each other.

Discussion of Results and Conclusions

A study of Tables 1–4 in the light of Eq. (10) shows that the major influence of δ and ε is on the nonrotating frequency. This factor also influences the third term in Eq. (10) through the factor f_2. The accuracy with which λ_n is estimated depends on the accuracy of the estimate of the nonrotating frequency of the Timoshenko beam. In the present case, exact solutions are used. For the Euler–Bernoulli beam ($\varepsilon = \delta = 0$) the contribution of the first term in Eq. (10) increases from 0 at α = 0 to 83% at α = 144. The second term contributes 100% at α = 0 and approximately 7% at α = 144. The contribution of the third term is approximately 10% to λ. For a Timoshenko beam with L/R = 10, the third term contributes approximately 98% to λ at α = 144. The second term has a negative contribution of 8.8% at α = 144, and the third term contributes 10.7% to λ.

The discrepancies between the results calculated from Eq. (10) and the exact values generally increase with increase in α and with decrease in L/R. As L/R decreases, the influence of shearing deformation becomes more important.

For n = 1, the maximum error is approximately 4% (for L/R = 10 and $\sqrt{\alpha}$ = 12) and for n = 2, the maximum error is less than 3%. For n = 3, the maximum error is less than 2%. For n = 4, the maximum error is 3.1%.

Equation (10) is similar in structure to the equation of Peters.[3] Even though the modifications introduced in deriving Eq.

(10) do not have a sound mathematical justification, the results are surprisingly accurate, not only for the fundamental frequency, but also for the overtone frequencies for a range of Timoshenko beams.

References

[1]Abramovich, H., and Elishakoff, I., "Influence of Shear Deformation and Rotary Inertia on Vibration Frequencies via Love's Equation," *Journal of Sound and Vibration*, Vol. 137, No. 3, 1990, pp. 516–522.

[2]Chandrasekhara, K., Krishna Murthy, K., and Roy, S., "The Vibration of Composite Beams Including Rotary Inertia and Shear Deformation," *Composite Structures*, Vol. 14, No. 4, 1990, pp. 269–279.

[3]Peters, D. A., "An Approximate Solution for the Free Vibration of Rotating Uniform Cantilever Beams," NASA TMX-62299, Sept. 1973.

[4]Stafford, R. D., and Giurgiutiu, V., "Semi-Analytic Methods for Rotating Timoshenko Beams," *International Journal of Mechanical Sciences*, Vol. 17, Nos. 11–12, 1975, pp. 719–727.

[5]Cowper, G. R., "The Shear Coefficient in Timoshenko's Beam Theory," *Journal of Applied Mechanics*, Vol. 33, June 1966, pp. 335–340.

Pitch Rate Effects on Delta Wing Vortex Breakdown

Lars E. Ericsson*
Mountain View, California 94040

Introduction

THE increasing performance demands on advanced aircraft, including maneuvers at high angles of attack, has led to a need for the prediction of vehicle aerodynamics that are dominated by unsteady separated flow effects. For aircraft with highly swept wing leading edges the challenge is to fully understand the unsteady flow physics behind the observed dramatic effects of vortex breakdown. In this Note, an attempt is made to pinpoint the fluid–mechanical processes that are causing the unpredicted large dynamic effects of high-rate/large-amplitude pitch oscillations on delta wing vortex breakdown.

Discussion

The pitching[1] and rolling[2] motions of delta wing aircraft have been found to have a large impact on the vortex breakdown characteristics. The fluid mechanics behind the surprisingly large pitch-rate-induced effects will be examined in what follows. The case of roll oscillations was analyzed in Refs. 3 and 4 for a 65-deg delta wing.

The vortex breakdown on a pitching 52-deg delta wing has been investigated by Atta and Rockwell[5] (Figs. 1 and 2). To quote the authors:

> There are several striking features of the vortex development and breakdown. First, the maximum extent of the laminar vortex core occurs near the maximum angle of attack (see photo C), rather than near the minimum angle of attack, which is in direct contradiction to what one would expect on the basis of quasisteady behavior.

Presented as Paper 95-0367 at the AIAA 33rd Aerospace Sciences Meeting and Exhibit, Reno, NV, Jan. 9–12, 1995; received Feb. 15, 1995; revision received Jan. 5, 1996; accepted for publication Jan. 10, 1996.

*Engineering Consultant. Fellow AIAA.

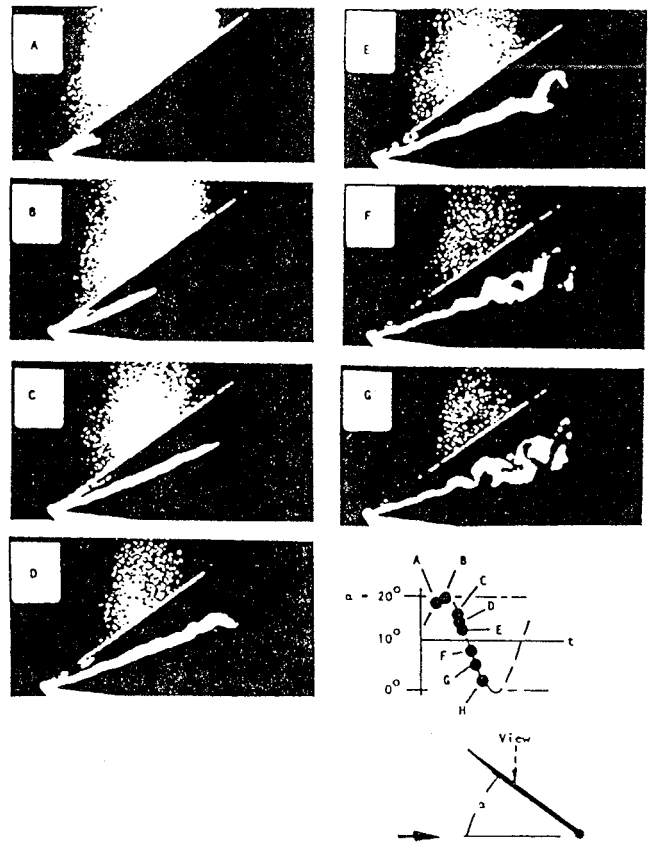

Fig. 1 Visualization of vortex breakdown on an oscillating 52-deg swept wing, $\alpha_0 = 10$ deg, $\Delta\alpha = 10$ deg, and $\bar{\omega} = 1.52$ (Ref. 5).

It is true that the local, instantaneous flow conditions, as defined in the classic quasisteady approach, cannot explain this dynamic deviation from the static vortex characteristics. However, it will be shown that when the definition of time-lagged, quasisteady characteristics used in Ref. 6 is extended to include the effects of rate-induced camber, the large dynamic effects in Figs. 1 and 2 can be explained. These dynamically equivalent steady (DES) characteristics, a nomenclature suggested by Beyers[7] to distinguish them from the classic quasisteady characteristics, will be described in what follows.

The classic, quasisteady (instantaneous) angle of attack is

$$\alpha = \alpha(t) - \dot{\alpha}(t)(x_{TE} - x)/U_\infty \tag{1a}$$

$$\alpha(t) = \alpha_0 + \Delta\alpha \sin \omega t \tag{1b}$$

$$\dot{\alpha}(t) = \Delta\alpha\omega \cos \omega t \tag{1c}$$

At the apex $x = x_A = 0$, and with $x_{TE} = c$, Eq. (1) gives

$$\alpha_A(t) = \alpha_0 + \Delta\alpha \sin \omega t - \Delta\alpha\bar{\omega} \cos \omega t \tag{2}$$

where, in the present case, $\alpha_0 = \Delta\alpha = 10$ deg and $\bar{\omega} = \omega c/U_\infty = 1.52$.

The development of a leading-edge vortex on the top side starts when the angle of attack at the apex exceeds $\alpha_A(t) = 0$. During the upstroke, $\dot{\alpha} > 0$, Eqs. (1) and (2) show that this value is reached when $\omega t = 23.2$ deg, where according to Eq. (1), $\alpha(t) = 13.9$ deg. The corresponding experimental value for $\xi = x/c = 0$ in Fig. 2 is $\alpha(t) = 17$ deg. According to Ref. 8, the difference between prediction and experiment could in part have been caused by the blunted 10-deg wedge shape of the leading edge. Another contributing cause is the following: Eq. (2) shows that $\alpha_A(t)$ starts at zero for $\omega t = -90$ deg, and reaches a peak negative value of -8.2 deg at $\omega t = -33.6$ deg and -5.2 deg at $\omega t = 0$, before finally reaching $\alpha_A(t) = 0$ at $\omega t = 23.2$ deg (Fig. 3). Thus, when $\alpha_A(t) > 0$ and leading-edge